POLITECNICO DI TORINO
Repository ISTITUZIONALE

Machine Learning-based Model for Defining Circuit-level Parameters of VCSEL

(Article begins on next page)

23 April 2024

Machine Learning-based Model for Defining Circuit-level Parameters of VCSEL

Ihtesham Khan
Politecnico di Torino, IT
ihtesham.khan@polito.it

Lorenzo Tunesi
Politecnico di Torino, IT
lorenzo.tunesi@polito.com

Muhammad Umar Masood
Politecnico di Torino, IT
muhammad.masood@polito.it

Enrico Ghillino
Synopsys, USA
enrico.ghillino@synopsys.com

Vittorio Curri
Politecnico di Torino, IT
curri@polito.it

Andrea Carena
Politecnico di Torino, IT
andrea.carena@polito.it

Paolo Bardella
Politecnico di Torino, IT
paolo.bardella@polito.it

Abstract—Recently, many computationally efficient models have been introduced to accurately define the static and dynamic Vertical Cavity Surface Emitting Laser (VCSEL) behaviors. However, in these models, many physical parameters must be appropriately set to reproduce existing laser sources' behavior accurately. The extraction of these unknown physical parameters from experimental curves is generally time-consuming and relies mainly on trial and error approaches or regression analysis, requiring extra effort. In this scenario, we propose a machine learning-based solution to the problem, which can effectively extract the required VCSEL parameters from experimental data in real-time. The proposed approach predicts the parameters exploiting the light-current curve and small-signal modulation responses with two steps at constant and variable temperature, respectively. Promising results are achieved in terms of relative prediction error.

Index Terms—Vertical Cavity Surface Emitting Lasers, Machine Learning, Parameters extraction, Circuit-level models, Deep Neural Network.

I. INTRODUCTION

Nowadays, lasers are used for a significant number of applications like information transmission, marking, cutting, drilling, additive manufacturing, etc. [1]–[6]. This unique number of applications is mainly due to the substantial flexibility of different tuning parameters, such as length of pulse, power, wavelength, and beam width. Nevertheless, this flexibility comes at the cost of a long set-up time and a considerable effort to locate the optimal parameters for each individual application. For instance, if you need to vary k parameters with N steps each, that corresponds to N^k tests. Additionally, the non-linear relationships among its parameters demand a generic systematic investigation of all possible combinations of the parametric space to pinpoint the optimal combination among them. However, this procedure is time-consuming, taking days or weeks, and unfocused, wasting energy, time, and money. In parallel, once this time-consuming procedure finds the optimal parametric combination, slight variations can change the optimal working point and hence demands another set of experimental trials to find a new combination of optimal parameters. In this scenario, a model is needed that identifies optimal parameters in real-time for different applications.

Typically, two broad classes of models are available for laser modeling; analytical and numerical treatment [7]. Analytical modeling generally centers around a single specific property of interest and related assumptions. In contrast, numerical modeling methodologies provide a general broad solution through approximation, but they are computationally expensive. This makes laser modeling extremely challenging for accurate and real-time characterization, thus putting the demand for alternative modeling solutions. In this context, Machine Learning (ML) has recently demonstrated itself as a potential substitute, having the ability to define an experimental model directly from experimental data. The ML-based models work in a complete agnostic way and only need a significant amount of data to model the lasers of different families, which are involved in various and diverse applications.

In the past few decades, different laser families have been introduced; VCSELs are among them, which are more complex due to their thermal and spatial characteristics. Recently, many computationally efficient models have been introduced to accurately define the static and dynamic VCSEL behaviors. These models play a fundamental role in understanding the VCSEL physical properties, allowing further optimizations of these devices. Along with this, they are also an essential resource for performing a realistic simulation of VCSEL sources as part of larger optoelectronic systems. Indeed, so-called "circuit-level models" of VCSEL are available in simulation tools such as Synopsys OptSim circuit simulation environment [8]. However, in these models, many physical parameters must be appropriately set to accurately reproduce the behavior of existing laser sources, which is a necessary step to obtain correct results from the numerical simulation of the whole photonic system. The extraction of these unknown physical parameters from experimental curves is generally time-consuming and relies on trial and error approaches or regression analysis. In this scenario, we propose an ML-based solution already applied for parametric extraction and inverse design problems of the laser [9]. The proposed ML-based solution to the problem enables the extraction of the required VCSEL parameters from experimental data effectively and has the potential to define the parameters in real-time. The
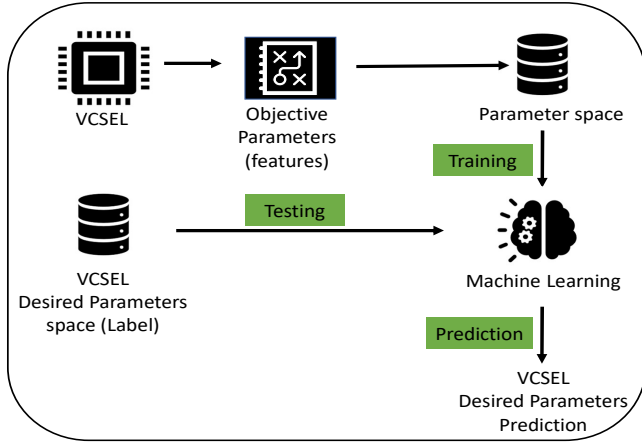
Fig. 1. ML assisted VCSEL parameters extraction.

$$\frac{\partial N_0}{\partial t} = \frac{\eta_i I}{q} - \frac{N_0}{\tau_n} - \frac{G\left[\gamma_{00}(N_0 - N_t) - \gamma_{01}N_1\right]}{1 + \varepsilon S}S - \frac{I_1}{q} \quad (1)$$

$$\frac{\partial N_1}{\partial t} = -\frac{N_1}{\tau_n}(1 + h_{diff}) + \frac{G\left[\phi_{100}(N_0 - N_t) - \phi_{101}N_1\right]}{1 + \varepsilon S} \quad (2)$$

$$\frac{\partial S}{\partial t} = -\frac{S}{\tau_p} + \frac{\beta N_0}{\tau_n} + \frac{G\left[\gamma_{00}(N_0 - N_t) - \gamma_{01}N_1\right]}{1 + \varepsilon S} \quad (3)$$

$$\frac{\partial \phi}{\partial t} = \frac{\alpha}{2}\frac{G\left[\gamma_{00}(N_0 - N_{tr}) - \gamma_{01}N_1\right]}{1 + \varepsilon S} \quad (4)$$

$$G(T) = G_0\left(a_{g0} + a_{g1}T + a_{g2}T^2\right) / \left(b_{g0} + b_{g1}T + b_{g2}T^2\right) \quad (5)$$

$$N_t(T) = N_{tr}\left(c_{n0} + c_{n1}T + c_{n2}T^2\right) \quad (6)$$

III. Dataset Generation using L-I and S_{21} Curves

The initial dataset of 10 000 simulations is generated at the constant temperature of 25 °C, varying the values of parameters reported in Tab. I and keeping all the other parameters fixed. During this dataset generation stage, all the parameters stated in Tab. II are set at their central value of the proposed ranges. In contrast, the remaining parameters are configured with the default values specified by OptSim. For each set of parameters, the dataset is filled with 16 samples of the calculated Light-Current (L-I) curve, generated for linearly spaced injected currents I ranging from 1 mA to 25 mA, an interval compatible with the considered parameter ranges. Also, small-signal modulation responses are calculated at 6 mA, 12 mA, 18 mA, and 24 mA; for each curve 16 samples are saved, for frequencies logarithmically spaced between 10 kHz and 50 GHz. An example of results used to fill the first dataset is shown in Fig. 2. Fig. 2 shows S-parameter small-signal modulation response (S_{21}) at different bias currents and fixed temperatures at 25 °C. These curves are numerically simulated switching on the device, waiting until stationary conditions are reached and then applying a 1% current amplitude step; a proper processing of the Fourier Transform of the output field [14] allows a simple estimation of the S_{21} curves.

The second dataset of 10 000 simulations is generated, using the data from four L-I curves calculated at 10 °C, 25 °C, 40 °C, and 55 °C; for each L-I curve 16 samples are stored shown in Fig. 3. Fig. 3 shows various curves at different temperatures, which generally let the modeling of the threshold current's temperature sensitivity and thermal rollover.

proposed solution is implemented in two steps, requiring training two ML agents on two different datasets. The first dataset is generated at a constant temperature, while the second dataset is generated at varying temperatures.

The rest of the article is divided into the following sections. Sec. II reports the description of the VCSEL model, while Sec. III illustrates how the datasets are generated for training the two ML agents. Sec. IV describes the detailed architecture of the proposed two ML agents. Finally, Sec. V reports the obtained promising results, followed by a brief conclusion.

II. Vertical Cavity Surface Emitting Lasers Model

The basic VCSEL block implemented inside OptSim contains a specific set of rate equations that take into consideration the thermal dependency of the gain and carrier leakage. Along with this, these equations also consider the spatial dependence of the carrier distribution and self-heating [10]. Furthermore, the VCESL building block implemented within OptSim also includes expressions for the cavity Current-Voltage (I-V) relationship and electrical parasitics.

The current work considered the VCSEL model accessible as a standard OptSim block. This implemented block is the extension of the model firstly proposed in [11] to incorporate the temporal evolution of the field phase [12]. In cylindrical geometry, the carrier number is expanded in the Bessel series, and the first two terms N_0 and N_1 are considered [13]. Assuming spatially independent rate equations, Eq.s 1-4 can be introduced for the temporal evolution of the carriers N_0 and N_1, the photons number S and the phase ϕ, with I injected current, q electron charge, I_1 leakage current, ϕ_{100} and ϕ_{101} overlap coefficient, β spontaneous emission coefficient, α linewidth enhancement factor. In order to model the dependence of the VCSEL behavior with respect to temperature T, a phenomenological representation of the gain G and the carrier transparency number N_t is introduced based on fitting parameters, as shown in Eq.s 5-6 [11]. Other parameters introduced in Eq.s (1-6), objective of the ML study and are finally defined in Tab. I and Tab. II.

Table I. Parameters investigated and variation ranges for generating 1st dataset at 25 °C. Last columns values are selected for generating 2nd dataset.

| Parameter	Range	Value
Current injection efficiency η_i	0.4 to 1	0.8
Photons lifetime τ_p	1.5 ps to 3.5 ps	2.5 ps
Carrier lifetime τ_n	1.5 ns to 3.5 ns	2.5 ns
Gain coefficient g_0	25 000 s^{-1} to 75 000 s^{-1}	50 000 s^{-1}
Carrier transparency number n_{tr}	0.5×10^6 to 1.5×10^6	1×10^6
Gain saturation factor ε	3×10^{-7} to 6×10^{-7}	5×10^{-7}
Overlap coeff. ($N_0 - S$) γ_{00}	0.75 to 1	1
Overlap coeff. ($N_0 - S$) γ_{01}	0.2 to 0.5	0.38
Diffusion parameter h_{diff}	7.5 to 22.5	15
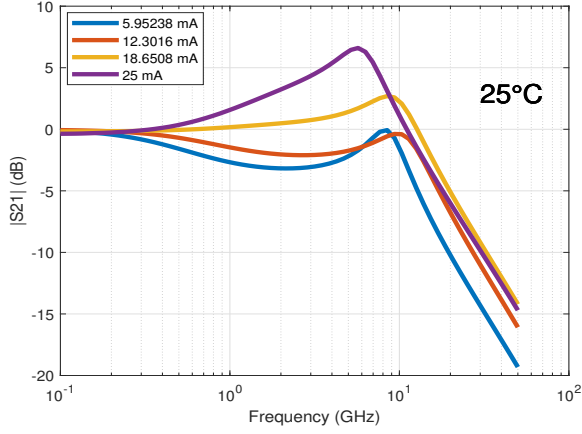
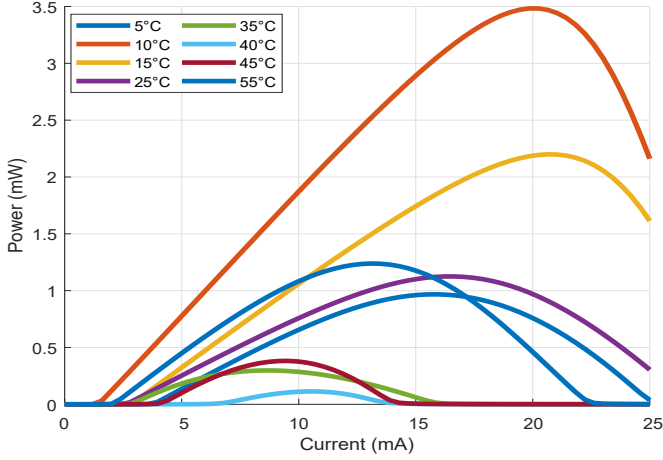Fig. 2. S_{21} curves calculated at varying current and fixed temperature 25 °C

Fig. 3. L-I curves calculated at varying temperature

Fig. 4. Parallel architecture of a deep neural network

IV. MACHINE LEARNING MODEL

The analysis proposed in this article mainly considers the extraction of 18 parameters listed in Tab. I and Tab.II. The extraction of 18 parameters using a single ML model is quite complex due to the difference between the characteristics of the two datasets, so the analysis is performed by simulating it in a two-step, which requires the training of two smaller ML agents mainly based on a Deep neural network (DNN) architecture having different numbers of hidden layers with ten neurons per layer [15]. The proposed DNN model used *ReLU* as an activation function and Mean square error (MSE)

Table II. Parameters investigated and variation ranges for generating the 2nd dataset.

Parameter	Range
Gain coeff. parameter a_{g0}	−0.6 to −0.2
Gain coeff. parameter a_{g1}	1×10^{-3} K^{-1} to 3×10^{-3} K^{-1}
Gain coeff. parameter a_{g2}	3×10^{-7} K^{-2} to 3×10^{-8} K^{-2}
Gain coeff. parameter b_{g0}	0.5 to 3
Gain coeff. parameter b_{g1}	-5×10^{-3} K^{-1} to -2×10^{-3} K^{-1}
Gain coeff. parameter b_{g2}	1×10^{-5} K^{-2} to 3×10^{-5} K^{-2}
Transparency number param. c_{n0}	−0.5 to −2
Transparency number param. c_{n1}	4×10^{-3} K^{-1} to 1.2×10^{-2} K^{-1}
Transparency number param. c_{n2}	3×10^{-6} K^{-2} to 1.2×10^{-5} K^{-2}

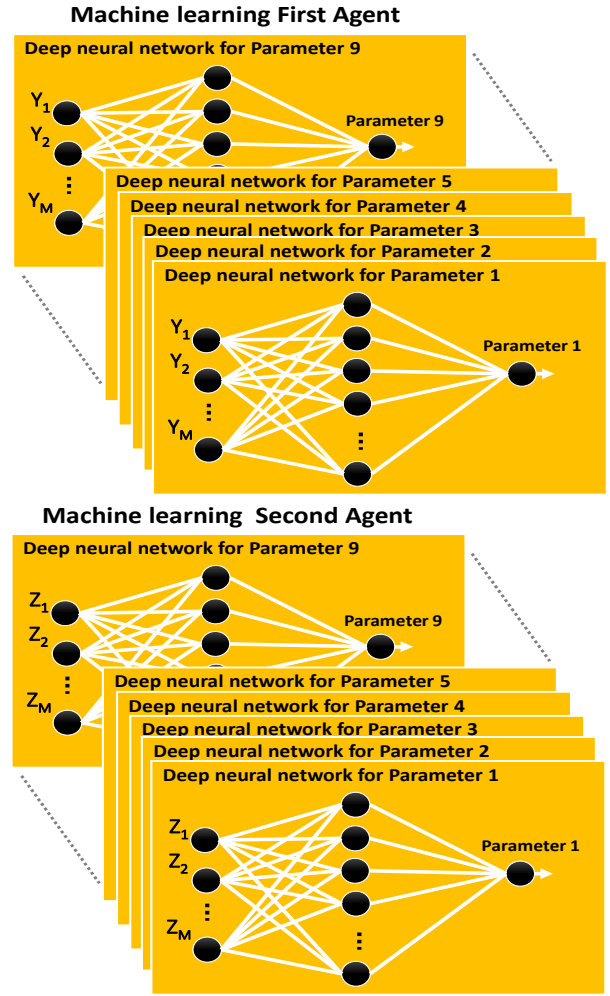as a loss function. The DNN model is configured for 1000 training steps with a default learning rate of 0.01. The training and test set proportion is 70% and 30% of the total dataset. The proposed DNN is developed by using a Deep Learning Toolbox™ of Matlab® platform. To improve the prediction efficiency, we propose a parallel architecture of the DNN for both the agents as shown in Fig. 4 [16]. For every VCSEL parameter, a single DNN unit is proposed to predict that specific parameter. To support this parallel DNN concept, a detailed analysis has been performed, which shows the MSE against the training steps keeping the number of neurons constant and varying the hidden layer size from 1 to 5 (see Fig. 5, Fig. 6). The Fig. 5, Fig. 6 show the first and the second agent MSE vs. training steps; it is pretty much visible that each of the DNN units proposed for predicting the given VCSEL parameters has different MSE values against the various configuration of hidden layer size. The hidden layer size that provides the minimum MSE is selected to get the superior predicting performance (represented by the dotted lines in Fig. 5 and Fig. 6). The first DNN agent is trained using a portion of data generated at a constant temperature (see Tab. I), and the other part of the same dataset is used
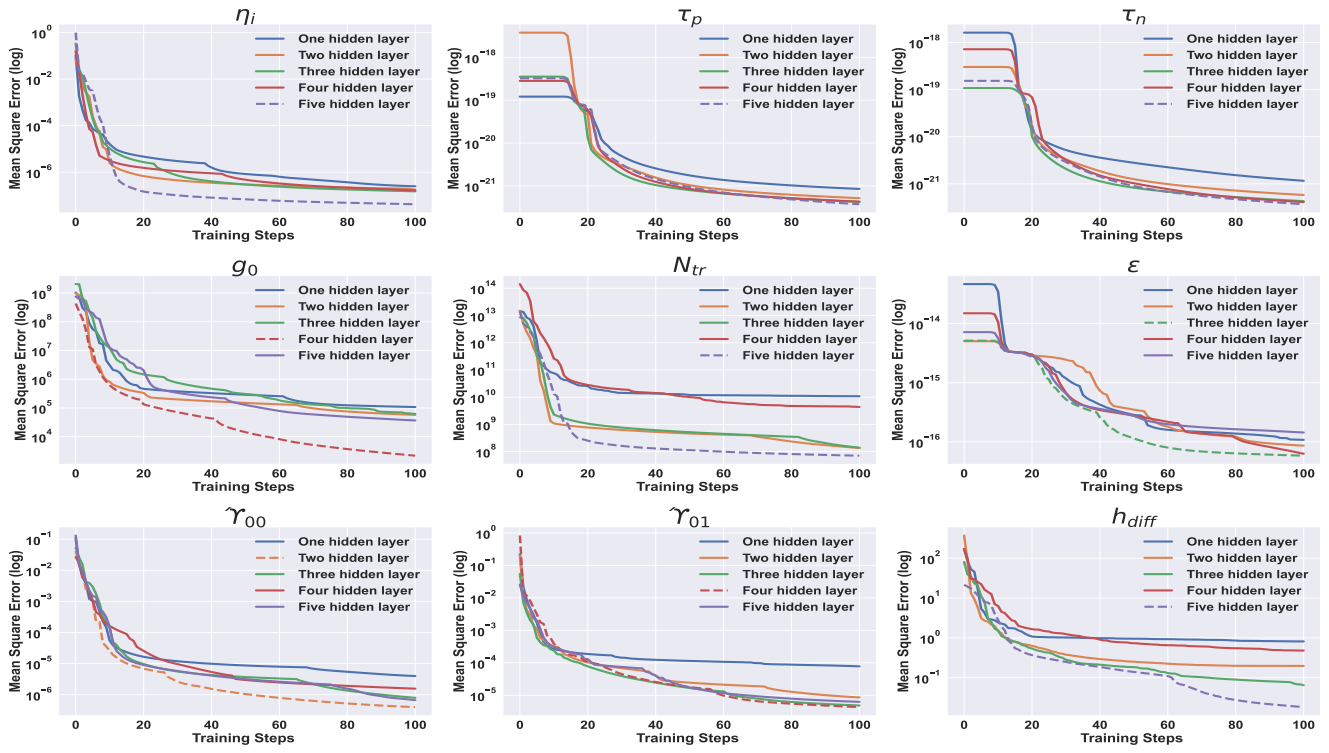
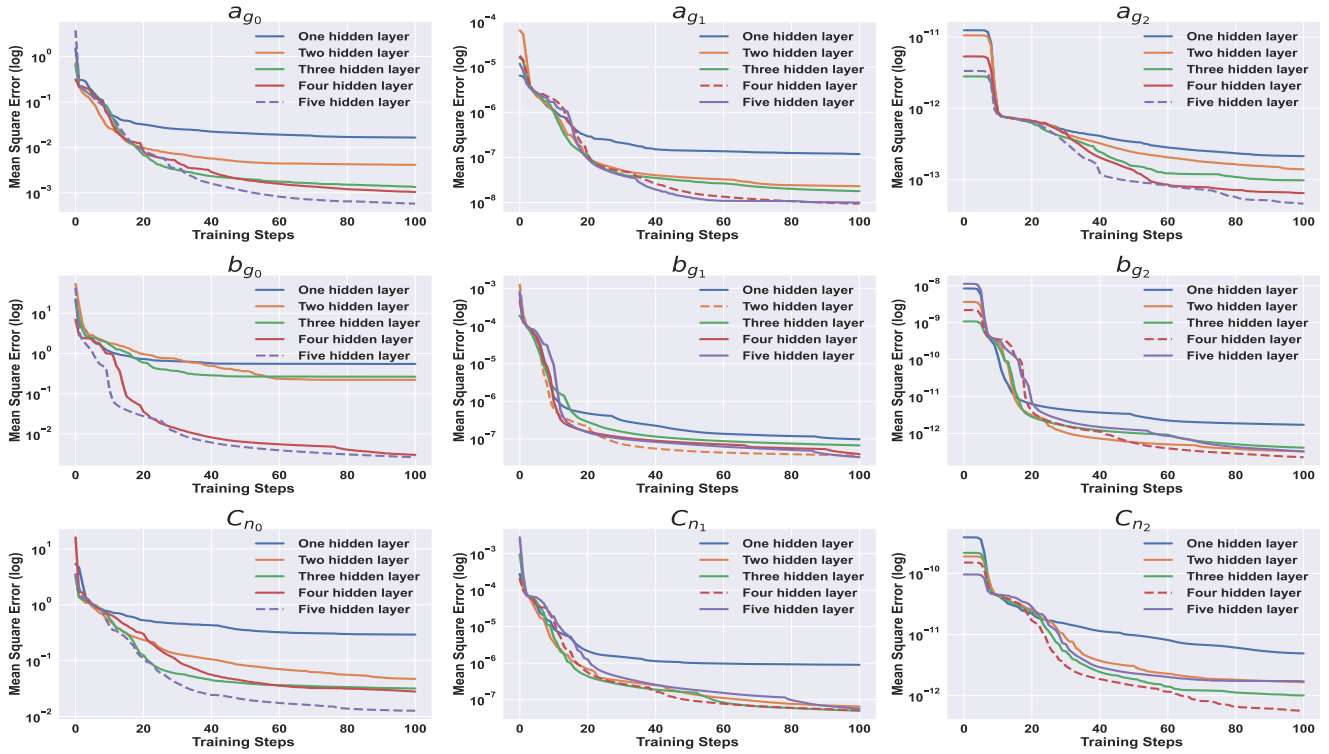Fig. 5. Mean Square Error of Ist agent for the 9 considered parameters.

Fig. 6. Mean Square Error of 2nd agent for the 9 considered parameters.
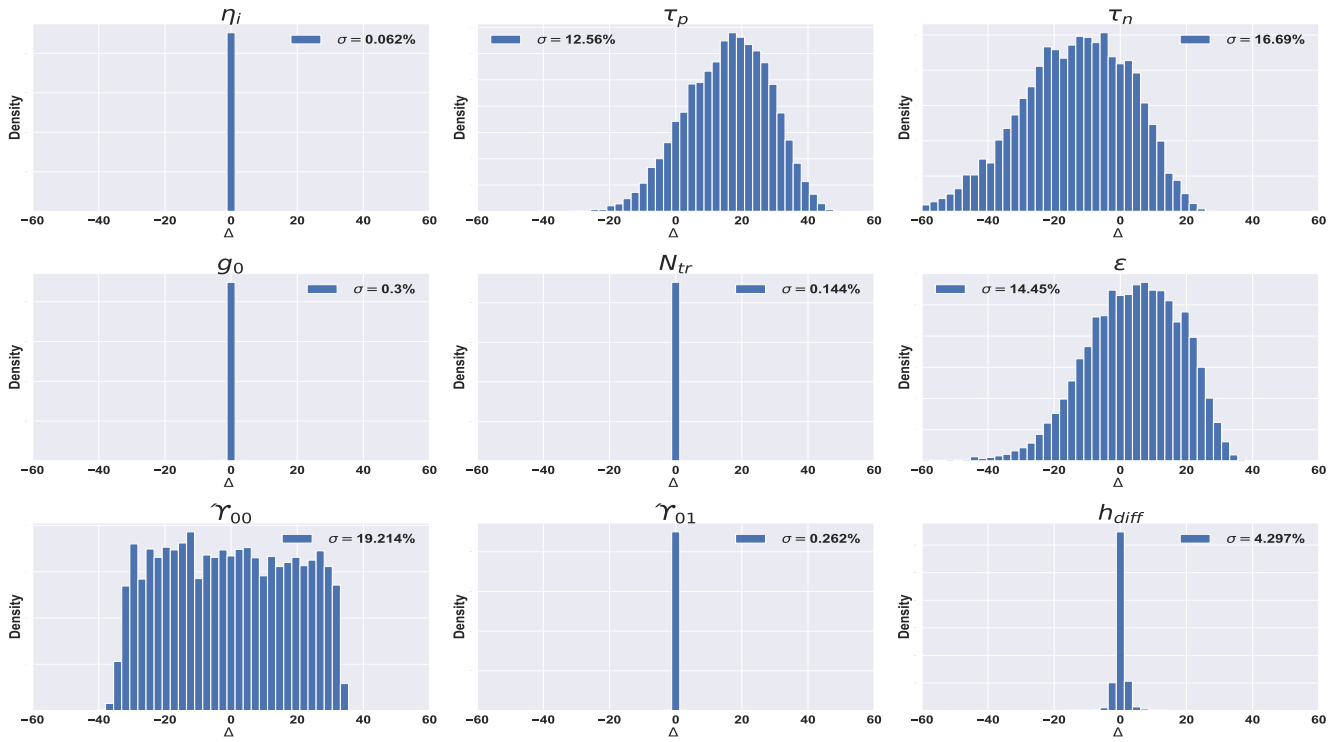
Fig. 7. Relative predicting error of 1st agent for the 9 considered parameters. Values in the titles of each histogram indicate the relative error standard deviation.
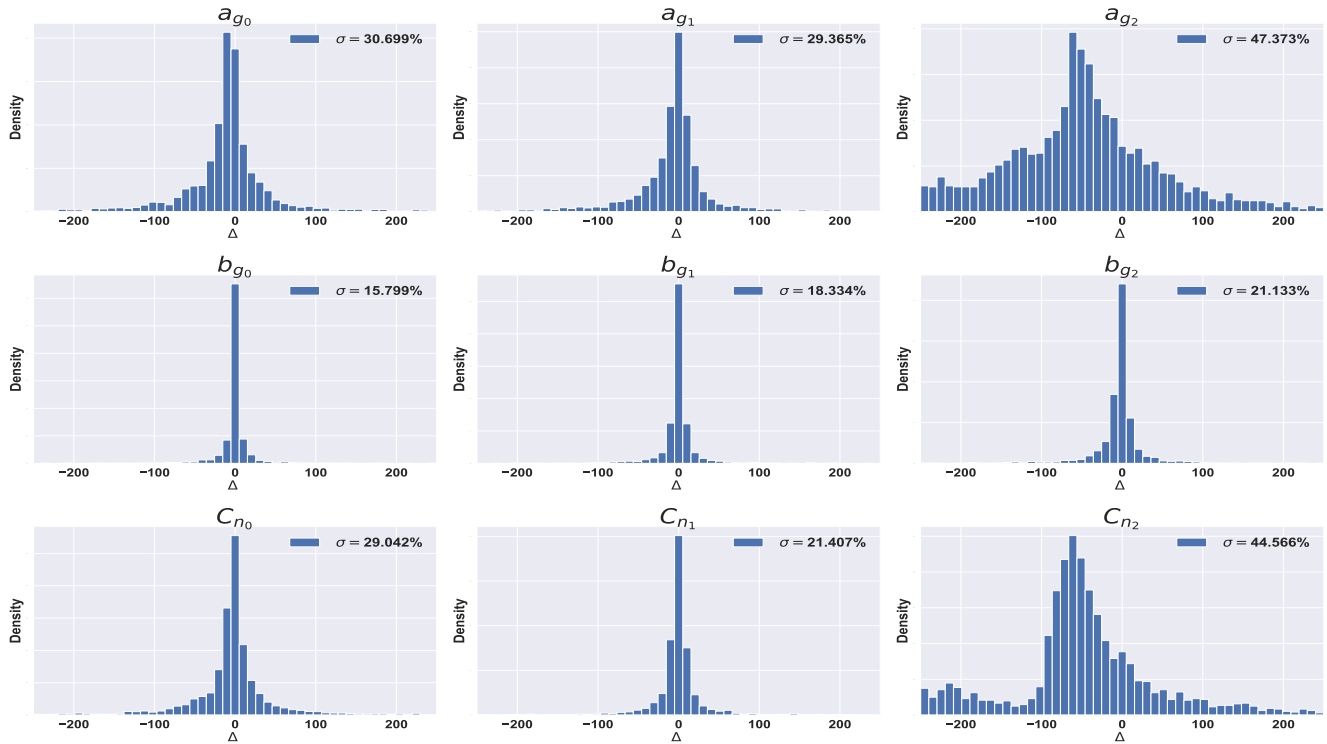

Fig. 8. Relative predicting error of 2nd agent for the 9 considered parameters. Values in the titles of each histogram indicate the relative error standard deviation.

to test the ML to extract these experimental data parameters reported in Tab. I while the second DNN agent is trained on a subset of another dataset of 10 000 simulations which are generated against varying temperature 10 °C, 25 °C, 40 °C, and 55 °C for each L-I curve. The other part of this second dataset is used to test the ML to extract the parameters reported in Tab. II

V. RESULTS

The predicting performance of each DNN unit is measured by the relative prediction error (Δ) of each considered parameter in the first and second test sets (see Eq. 7). The results related to first ML agent and second ML agent are presented in Fig. 7 and Fig. 8, respectively. Fig. 7 and Fig. 8 show the histogram of relative error of the considered parameters along with the relative error standard deviation. Along with this, for all the evaluated parameters, the corresponding MSE at the end of the training is less than 0.1.

$$\Delta = \frac{Predicted\,Value - Actual\,Value}{Actual\,Value} \qquad (7)$$

Generally, high-level accuracy is obtained for the 9 parameters of the first dataset related to the first ML agent. In contrast, the prediction accuracy is decreased for the second dataset associated with the second ML agent; this is mainly because some of the parameters introduce the temperature dependence, such as a_{g2} and c_{n2}. However, the later coefficients introduce a second-order dependence with temperature, which causes limited effects over the considered temperature range, and are therefore difficult to estimate. The proposed model can quickly obtain an accurate set of VCSEL parameters through a fully automatized and agnostic process. The total simulation requires approximately a few hours of computation to generate the datasets and train the ML agents, running on the latest workstations. Moreover, in a more complex application, the proposed model can be easily scaled up with a good level of accuracy for a larger number of parameters (with respect to the current 18 analyzed in this work) because of its parallel architecture that has the capability to be swiftly expanded without affecting the accuracy, which empowers the proposed architecture to be positively adapted for studying other laser classes.

VI. CONCLUSION

In the current era, lasers are used for many applications in industries and academia. This massive usage of lasers is mainly due to the flexibility of different tuning parameters that enable them to adapt to various applications quickly. However, this flexibility is achieved at the cost of a long time and a considerable effort paid to find the optimal parameters for each particular application. In this scenario, we proposed a machine learning-based framework which can effectively extract the required VCSEL parameters from experimental data. The proposed approach can extract an accurate set of 18 VCSEL parameters in real-time through a fully automated way. Besides this, the presented method can be easily expanded to a larger

number of parameters in more complex models and can be definitely adapted for characterizing other laser families.

REFERENCES

[1] J. Diaci, D. Bračun, A. Gorkič, and J. Možina, "Rapid and flexible laser marking and engraving of tilted and curved surfaces," *Opt Lasers Eng* **49**, 195–199 (2011).

[2] J. Qi, K. Wang, and Y. Zhu, "A study on the laser marking process of stainless steel," *J. Mater. Process. Technol.* **139**, 273–276 (2003). IMCC2000 Vol. 2 S.I.

[3] M. Moradi, O. Mehrabi, T. Azdast, and K. Y. Benyounis, "Enhancement of low power CO2 laser cutting process for injection molded polycarbonate," *Opt. Laser. Technol.* **96**, 208–218 (2017).

[4] K. Salonitis, A. Stournaras, G. Tsoukantas, P. Stavropoulos, and G. Chryssolouris, "A theoretical and experimental investigation on limitations of pulsed laser drilling," *J. Mater. Process. Technol.* **183**, 96–103 (2007).

[5] G. Scotti, V. Matilainen, P. Kanninen, H. Piili, A. Salminen, T. Kallio, and S. Franssila, "Laser additive manufacturing of stainless steel micro fuel cells," *J. Power Sources* **272**, 356–361 (2014).

[6] E. Akman, A. Demir, T. Canel, and T. Sınmazçelik, "Laser welding of ti6al4v titanium alloys," *J. Mater. Process. Technol.* **209**, 3705–3713 (2009).

[7] P. Parandoush and A. Hossain, "A review of modeling and simulation of laser beam machining," *Int. J. Mach. Tools Manuf.* **85**, 135–145 (2014).

[8] https://www.synopsys.com/photonic-solutions/pic-design-suite.html.

[9] Z. Ma and Y. Li, "Parameter extraction and inverse design of semiconductor lasers based on the deep learning and particle swarm optimization method," *Opt. Express* **28**, 21971–21981 (2020).

[10] G. Sialm, D. Lenz, D. Erni, G.-L. Bona, C. Kromer, M. X. Jungo, T. Morf, F. Ellinger, and H. Jckel, "Comparison of simulation and measurement of dynamic fiber-coupling effects for high-speed multimode VCSELs," *J. Lightwave Technol.* **23**, 2318 (2005).

[11] P. Mena, J. Morikuni, S.-M. Kang, A. Harton, and K. Wyatt, "A comprehensive circuit-level model of vertical-cavity surface-emitting lasers," *J. Light. Technol.* **17**, 2612–2632 (1999).

[12] M. X. Jungo, D. Erni, and W. Bachtold, "VISTAS: a comprehensive system-oriented spatiotemporal VCSEL model," *IEEE J. Sel. Top. Quantum Electron.* **9**, 939–948 (2003).

[13] P. Mena, J. Morikuni, and K. Wyatt, "Compact representations of mode overlap for circuit-level VCSEL models," (2000), pp. 234–235 vol.1.

[14] P. Bardella, W. W. Chow, and I. Montrosset, "Design and analysis of enhanced modulation response in integrated coupled cavities DBR lasers using photon-photon resonance," *Photonics* **3** (2016).

[15] I. Khan, L. Tunesi, M. U. Masood, E. Ghillino, P. Bardella, A. Carena, and V. Curri, "A neural network-based automatized management of N× N integrated optical switches," in *Photonic Networks and Devices,* (OSA, 2021), pp. NeF2B–2.

[16] I. Khan, L. Tunesi, M. U. Masood, E. Ghillino, P. Bardella, A. Carena, and V. Curri, "Machine learning driven model for software management of photonics switching systems," in *2021 IEEE Global Communications Conference (GLOBECOM),* (IEEE, 2021), pp. 1–6.